Model of electron pressure anisotropy in the electron diffusion region of collisionless magnetic reconnection

Cite as: Phys. Plasmas **17**, 122102 (2010); https://doi.org/10.1063/1.3521576
Submitted: 14 September 2010 . Accepted: 27 October 2010 . Published Online: 15 December 2010

A. Divin, S. Markidis, G. Lapenta, V. S. Semenov, N. V. Erkaev, and H. K. Biernat

Model of electron pressure anisotropy in the electron diffusion region of collisionless magnetic reconnection

A. Divin,[1,a)] S. Markidis,[1] G. Lapenta,[1] V. S. Semenov,[2] N. V. Erkaev,[3] and H. K. Biernat[4]
[1]*Centrum voor Plasma-astrofysica, Katholieke Universiteit Leuven, B-3001 Heverlee, Belgium*
[2]*Department of Physics, St. Petersburg State University, St. Petersburg 198504, Russia*
[3]*Institute for Computational Modelling, Russian Academy of Sciences, Krasnoyarsk 660036, Russia and Siberian Federal University, Krasnoyarsk 660041, Russia*
[4]*Space Research Institute, Austrian Academy of Sciences, Graz A-8042, Austria and Institute of Physics, University of Graz, Graz A-8010, Austria*

(Received 14 September 2010; accepted 27 October 2010; published online 15 December 2010)

A new model of the electron pressure anisotropy in the electron diffusion region in collisionless magnetic reconnection is presented for the case of antiparallel configuration of magnetic fields. The plasma anisotropy is investigated as source of collisionless dissipation. By separating electrons in the vicinity of the neutral line into two broad classes of inflowing and accelerating populations, it is possible to derive a simple closure for the off-diagonal electron pressure component. The appearance of these two electron populations near the neutral line is responsible for the anisotropy and collisionless dissipation in the magnetic reconnection. Particle-in-cell simulations verify the proposed model, confirming first the presence of two particle populations and second the analytical results for the off-diagonal electron pressure component. Furthermore, test-particle calculations are performed to compare our approach with the model of electron pressure anisotropy in the inner electron diffusion region by Fujimoto and Sydora [Phys. Plasmas **16**, 112309 (2009)]. © *2010 American Institute of Physics*. [doi:10.1063/1.3521576]

I. INTRODUCTION

Magnetic reconnection is one of the most important energy conversion processes in space, astrophysical and laboratory plasmas.[1,2] It is responsible for explosive phenomena, such as solar flares, magnetospheric substorms, and tokamak disruptions. Magnetic reconnection is essentially a dissipative process. Dissipation is typically localized to a tiny region, the so-called diffusion region (DR). The idea of diffusion region is inherently related to the notion of magnetic field lines that are frozen into plasma. In a magnetized plasma, if particle collisions are neglected, particles are tied to a particular flux tube. Typical motions are the Larmor gyration and the $\mathbf{E}\times\mathbf{B}$ drift. Dissipation enables the breaking and rearranging of the magnetic field lines that pull particles away from the flux tube. Dissipative processes are represented by additional "nonideal" terms in the froze-in constraint equation. The famous models by Sweet[3] and Parker[4] rely on the presence of a uniform resistivity arising from particle collisions. Although the basic principles of the models are confirmed by numerical and experimental studies,[1] their direct application to events, such as solar flares and magnetospheric substorms, predicted the events to be much slower than the observed time scales.[1,3,4] Because of the very low collision rate in such environments, the investigation of the resistivity enhancement turned to the study of kinetic-scale collisionless processes.

Various mechanisms of collisionless dissipation within the diffusion region are proposed. Among them, there are turbulence, kinetic instabilities,[5,6] chaotization of particle trajectories,[7,8] and finite bulk flow inertia within the DR.[9,10] The demagnetization of particles close to neutral line makes acceleration by the transversal electric field possible. Strong particle acceleration and heating, leading to non-Maxwellian plasma distribution functions,[11,12] are found in the DR.[13,14] Thus, the pressure becomes anisotropic and all the pressure tensor components should be considered.

Vlasov and particle-in-cell (PIC) simulations advanced significantly the understanding of magnetic reconnection. In fact, kinetic processes were found to create substantial dissipation to make reconnection fast. Magnetic reconnection develops a multiscale structure with different dynamics of electrons and ions in the simple two-dimensional case with inflowing antiparallel magnetic fields and the third direction ignored. The ion diffusion region (IDR) thickness is around the ion inertial length d_i or thermal gyroradius in ambient magnetic field ρ_i. The IDR length is estimated to be more than $10d_i$. The electron diffusion region (EDR) is embedded within the IDR whose width scales similarly[1,15] with the electron skin depth d_e or electron thermal gyroradius ρ_e. The length of the EDR is a subject of recent controversy: electrons are unmagnetized over large distances larger than $10d_i$ within a narrow jet in the outflow direction,[16,17] and claimed to be at least $60d_i$ in the magnetopause reconnection.[18] This flow was later called "reconnection ejecta" and marks the area of the "external EDR," while the part of EDR immediately adjacent to neutral line, where the dissipative electric field dominates, was designated as "inner EDR."[17,19,20] We investigate the properties of the pressure anisotropy in the inner EDR. This requires the study of the off-diagonal component P_{yz} of the pressure tensor (in frames of reference used

a)Electronic mail: andrey.div@gmail.com.

in Refs. 15, 17, and 19–21) close to the neutral line for the case of antiparallel magnetic reconnection.

The pressure term appears directly in the electron equation of motion in the form of $\nabla\cdot\mathbf{P}_e$. This term balances the electric field, together with the bulk flow inertia and convection term. The bulk flow stagnates within the inner EDR, and the $\nabla\cdot\mathbf{P}_e$ term could balance the reconnection electric field if sufficient plasma anisotropy is developed here.[21] The mechanism of dissipation in the collisionless laminar case, based on thermal inertia and pressure anisotropy, was first introduced by Vasyliunas[21] and later developed by Dungey.[22] Test-particle calculations[23,24] and PIC simulations[15,17,25–27] confirmed the appearance of a large electron pressure anisotropy within the EDR as the main mechanism for breaking the froze-in constraint in such collisionless configurations.

The goal of this study is to examine the underlying physics of the electron pressure anisotropy in the inner EDR. A thorough comparison with PIC simulations as well as with the model of the pressure anisotropy inside the EDR developed by Fujimoto and Sydora[28] is performed.

The article is organized as follows:

- First, we derive a simple expression for the off-diagonal component of the electron pressure tensor near the neutral line. For this derivation, the properties of particle trajectories in the field-reversal are discussed.
- Second, PIC simulations verify the proposed electron pressure anisotropy model. A procedure for categorizing different trajectories is used additionally to divide particles of different classes (magnetized or unmagnetized).
- Third, we use the test-particle approach to study the model by Fujimoto and Sydora[28] and point out the properties and similarities with our model. The transition from the Fujimoto and Sydora model into the one developed in this paper is discussed.

II. ELECTRON PRESSURE ANISOTROPY MODEL

The derivation of the off-diagonal component of the electron pressure P_{yz} near the neutral line of antiparallel collisionless magnetic reconnection is presented in this section.

A. Preliminary considerations

The simplifications assumed in our derivation are described first. The following configuration is used: the magnetic field $\mathbf{B}$ at the EDR inflow edge is directed in the $\hat{\mathbf{x}}$ direction, the magnetic field in the outflow region is in the $\hat{\mathbf{y}}$ direction, and the reconnection electric field is in the $\hat{\mathbf{z}}$ direction.

Several important assumptions are made.[28–30] First, plasma is collisionless, thus no resistivity is present and all the dissipation arises from particle thermal inertia (see two-dimensional simulations[15,17,19]). Second, reconnection is in the steady state, thus the electric field component E_z is constant and uniform around the X-line, up to all relevant kinetic scales at least (ion and electron inertial lengths d_i and d_e being, respectively, typical transversal scales of the IDR and inner EDR). A significant scale separation between electrons and ions is present, with the ion dynamics being negligible inside the EDR. Both ions and electrons are magnetized in the inflow region.[15] Particles experience a $\mathbf{E}\times\mathbf{B}$ drift in the direction of the outflow region there. The Hall term-related physics is important within $d_e \lesssim y \lesssim d_i$, because the magnetic field is frozen here into the motion of electron component of plasma only. Several fluid models[31–33] (i.e., Hall MHD or electron Hall MHD) successfully describe this region.

Electrons are demagnetized within $y<d_e$ near the X-line and accelerated by E_z, leading to anisotropic distribution functions. Nonzero values of $(\nabla\cdot\mathbf{P}_e)_z$ are created mostly by the $\partial P_{yz}/\partial y$ term.[17,19,20] The evolution of all components of anisotropic pressure tensor $\mathbf{P}$ could be resolved by taking the second order moments of the Boltzmann equation.[34] If the contribution from heat flux tensor Q_{ijk} is omitted, the equation for $\partial\mathbf{P}/\partial t$ can be written[27,30] in the closed form via the pressure $\mathbf{P}$, the bulk flow velocity $\mathbf{v}$, and the specie density n.

Another way to analyze the properties of an unmagnetized electron fluid is to study the electron trajectories in field-reversals. Because the plasma is collisionless and short-range interparticle forces are neglectable, the motion of particles depends only on the global configuration of the magnetic and electric fields. Theoretical models approximate the magnetic field as an elongated X-line with hyperbolic magnetic potential close to the neutral line. Moreover, the electric field is assumed uniform and constant. The integration of the trajectories provides an estimate of the average velocity and of the trapping time within the field-reversal, together with other relevant scalings.[1,35–37] This approach is adopted in this paper. The properties of particle trajectories are revisited first, and the approximate expressions for the anisotropic pressure component P_{yz} are then derived.

B. Particle trajectories in the EDR

Following the examples of Refs. 1 and 35–37, the magnetic field is taken in the form of elongated X-line configuration inside the EDR. The X-line is parallel to the $\hat{\mathbf{z}}$ axis and passes through the points $x=0$, $y=0$. The magnetic potential is $A_y=\frac{1}{2}(B_{x0}y^2/\delta - B_{y0}x^2/L)$ with the EDR width δ much smaller than the EDR length L. The magnetic field is simply $\mathbf{B}=\hat{\mathbf{x}}B_{x0}y/\delta+\hat{\mathbf{y}}B_{y0}x/L$. Here we state that $B_x=B_{x0}$ at the inflow EDR edge (at $y=\pm\delta$) and $B_y=B_{y0}$ at the outflow edge (at $x=\pm L$). The electric field is $\mathbf{E}=\hat{\mathbf{z}}E_z$. Then we recall the equation of motion in the form of

$$\frac{dv_x}{dt}=-\frac{q}{m_e c}v_z B_y; \quad \frac{dv_y}{dt}=\frac{q}{m_e c}v_z B_x, \tag{1}$$

$$\frac{dv_z}{dt}=\frac{q}{m_e}E_z+\frac{q}{m_e c}(v_x B_y - v_y B_x). \tag{2}$$

We assume that the influence of magnetic field in Eq. (2) is smaller than the acceleration by the electric field for the largest part of a particle trajectory within the EDR. Thus, the solution for v_z is simply[1] $v_z \approx eE_z t/m_e + \text{const}$. Equation (1) is cast in the usual form of Airy equations,

$$\frac{dv_x}{dt}=-\frac{e^2E_z}{cm_e^2}\frac{B_{y0}}{L}xt, \tag{3}$$

$$\frac{dv_y}{dt} = \frac{e^2 E_z}{cm_e^2}\frac{B_{x0}}{\delta} yt. \tag{4}$$

For $E_z<0$, being a proper sign reconnection electric field for the configuration $B_x<0$ $(x<0)$, $B_x>0$ $(x>0)$, the exact solution is represented by the Airy functions for Eq. (3) and by Airy functions of negative argument for Eq. (4).

The acceleration time scale τ_{0x} of a particle before it is diverted by the reconnected magnetic field is[1] the time scale of Eq. (3),

$$\tau_{0x} = \left(\frac{m_e^2 cL}{e^2|E_z|B_{y0}}\right)^{1/3}, \tag{5}$$

and the estimate for the typical v_z particle velocity inside the EDR[1,13,37] is

$$v_z \cong \frac{e}{m_e}E_z\tau_0 = \left(\frac{ecLE_z^2}{mB_{y0}}\right)^{1/3}. \tag{6}$$

The period of the meandering motion is estimated as

$$\tau_{0y} = \left(\frac{m_e^2 c\delta}{e^2|E_z|B_{x0}}\right)^{1/3}. \tag{7}$$

According to a common picture of reconnection with X-line being elongated in the direction of the outflow, we have $B_{y0}\ll B_{x0}$ and $\delta\ll L$, and therefore[37] $\tau_{0y}\ll\tau_{0x}$. The ejection of particles along the $\hat{\mathbf{x}}$ axis is combined with the much faster meandering motion within the EDR in the $\hat{\mathbf{y}}$ direction. The solution of Eq. (4),

$$y = c_1 Ai\{-t/\tau_{0y}\} + c_2 Bi\{-t/\tau_{0y}\}, \tag{8}$$

represents damped oscillations and is approximated by $y\sim t^{-1/4}\sin\left[\frac{2}{3}(t/\tau_{0y})^{3/2}+\pi/4\right]$ for large t. The factor of the amplitude decay $(t^{-1/4})$ is relatively small. In view of all other uncertainties,[14] we approximate the whole population of accelerated particles as a flow with bulk velocity v_z [see Eq. (6)]. Details can be found in a textbook.[1]

C. P_{yz} estimate

The previous analysis and discussion show that the main physical process that contributes to electron pressure anisotropy tensor near the X-line is the acceleration of the inflowing electrons into EDR by the reconnection electric field. Because the boundary between the inflow and accelerated plasmas is smoothed, the distribution function $f_e(\mathbf{v},\mathbf{r})$ at the top and at the bottom of the EDR inflow edge is composed of the following:

- $f_a(\mathbf{v},\mathbf{r})$—distribution function of accelerated (a) meandering particles, moving with large v_z velocity;
- $f_d(\mathbf{v},\mathbf{r})$—distribution function of magnetized particles, drifting (d) into the EDR with small $v_y<0$ $(y>0)$ and $v_y>0$ $(y<0)$.

Hence, the electron distribution function f_e can be approximated as $f_e=f_a+f_d$. We assume some rather general properties of the inflowing and accelerated populations. The inflow particles are assumed to have an initial temperature which makes the distribution function $f_d(\mathbf{v},\mathbf{r})$ to be an even function with respect to v_z,

$$f_d(-v_z) = f_d(v_z). \tag{9}$$

Moreover, the accelerated population is assumed to be symmetric in the v_y direction,

$$f_a(-v_y) = f_a(v_y), \tag{10}$$

since the thermal spread and fluctuations disperse the meandering particles in the v_y velocity space.

We define the mean value of a quantity F as usual,

$$\langle F\rangle_k = \frac{1}{n_k}\int F(\mathbf{v})f_k(\mathbf{v},\mathbf{r})d\mathbf{v}, \tag{11}$$

$$n_k = \int f_k(\mathbf{v},\mathbf{r})d\mathbf{v}, \tag{12}$$

where $k=e,a,d$ denotes the total, accelerated, and inflowing populations.

The suggested symmetry properties of the distribution functions f_a and f_d lead to the relation $\langle v_y v_z\rangle_e=0$. The off-diagonal term P_{yz} of the electron pressure tensor results to

$$P_{yz} = m_e\int (v_y-\langle v_y\rangle)(v_z-\langle v_z\rangle)f_e)d\mathbf{v} = m_e\int v_y v_z f_e d\mathbf{v} - m_e n_e\langle v_y\rangle_e\langle v_z\rangle_e = -m_e n_e\langle v_y\rangle_e\langle v_z\rangle_e. \tag{13}$$

Moreover, the equality $\langle v_y v_z\rangle_e=0$ will be sufficient to make the expression (13) correct even if conditions (9) and (10) are relaxed.

Considering that $n_e=n_a+n_d$, $n_e\langle v_y\rangle_e=n_d\langle v_y\rangle_d$, and $n_e\langle v_z\rangle_e=n_a\langle v_z\rangle_a$, another representation in terms of the accelerated and inflow populations can be derived,

$$P_{yz} = -m_e\frac{n_a n_d}{n_a+n_d}\langle v_y\rangle_d\langle v_z\rangle_a. \tag{14}$$

Expressions (13) and (14) reflect all the typical properties of P_{yz} inside the DR: in fact, near the edge, $n_a\to 0$, and therefore $P_{yz}\to 0$; at the stagnation point at $y\sim 0$, $\langle v_y\rangle_e\sim 0$, and therefore $P_{yz}\to 0$. Accordingly, P_{yz} has a peak within the EDR. This is in agreement with the usual view of $P_{yz}(y)$ as an odd function[21] with respect to y.

These expressions provide a pressure anisotropy estimate at the DR inflow edge. The reconnection electric field is then given by

$$|E_z| \cong (1/en_e)P_{yz}/\delta = m_e\langle v_y\rangle_e\langle v_z\rangle_e/(e\delta). \tag{15}$$

The expressions (13) and (14) are similar to the results of Fujimoto and Sydora,[28] but are obtained using considerably different approximations to the structure of distribution functions in the inner EDR and assuming their specific symmetry properties [Eqs. (9) and (10)]. This finding is interesting since the model[28] assumes that all particles undergo meandering oscillations. It cancels out bulk flow velocity, $\langle v_y\rangle_e=0$, thus $m_e n_e\langle v_y\rangle_e\langle v_z\rangle_e=0$ and the pressure anisotropy is supported by the $m_e n_e\langle v_y v_z\rangle_e$ term. The effective velocity of the meandering motion in the $\hat{\mathbf{y}}$ direction is taken instead of

the $\langle v_y \rangle_e$, which roughly represents the velocity of the inflowing particles. Hence, the final equations of both models are similar: Eqs. (13) and (14) of the present article and Eqs. (13) and (14) of Ref. 28.

In the next section, we confirm our estimates of the pressure anisotropy [Eqs. (13) and (14)] and discuss the applicability of the $\langle v_y v_z \rangle_e = 0$ approximation.

III. COMPARISON WITH PIC SIMULATION RESULTS

The results of PIC simulations of magnetic reconnection are presented to show that distribution functions used to derive expressions (13) and (14) in fact appear in the EDR. Calculations use the full-particle implicit code iPic3D.[38,39] The implicit moment PIC method[40] allows a significant reduction of the required computational resources and is capable of realistic mass-ratio simulations. However, our calculations are restricted to the case of $m_e/m_i = 1/256$ to ensure higher resolution of the EDR. A Harris-type current sheet[41] is taken as initial condition,

$$B_x(y) = B_0 \tanh\frac{y}{L}, \quad n_s(y) = n_0 \cosh^{-2}\frac{y}{L} + n_b, \quad s = e,i. \tag{16}$$

The background plasma density is $n_b = 0.2 n_0$. Temperature ratio is $T_i/T_e = 5$ with background and current sheet plasma temperature equal at $t=0$. The ratio of the ion Alfvén velocity V_a to the speed of light c is $V_a/c = 0.0097$. The thickness of the initial current sheet is $L = 0.5 d_i$. A small initial non-GEM (Ref. 39) perturbation is added to start reconnection,

$$\Psi(x,y) = \Psi_0 \cos\frac{2\pi(x - L_x/2)}{L_x} \cos\frac{\pi y}{L_y} e^{-[(x - L_x/2)^2 + y^2]^2/\sigma^2}, \tag{17}$$

where $\mathbf{B}' = \nabla \times \Psi(x,y)\hat{\mathbf{z}}$. The intensity Ψ_0 is 0.1, and range σ is $1 d_i$. The computational domain size L_x is $30 d_i$ and L_y is $15 d_i$, and resolution $\Delta x = d_i/48 = d_e/3$. Periodic boundary conditions are used in the $\hat{\mathbf{x}}$ direction; perfect electric conductor boundaries are set at $y = -L_y/2$ and $y = L_y/2$.

Reconnection starts after the X-line perturbation introduces a small deviation from the equilibrium force-balance. By time $\Omega_{i0} t \sim 26.1$, the initial current sheet is reconnected and the evolution turns quasistationary in proximity of the EDR. On the other hand, $\Omega_{i0} t \sim 26.1$ is small enough to avoid the influence of periodic boundary conditions and of stagnation, because the reconnected magnetic flux is trapped inside the computational domain. That particular time is chosen to analyze the distribution functions and the electron anisotropy. Here Ω_{i0} is ion cyclotron frequency in ambient magnetic field.

The reconnection rate is $M_e \sim 0.15$. A comparable value is obtained in the other fast reconnection studies.[1,15] We revisit briefly the kinetic Ohm's law to confirm the properties of plasma flow (see Fig. 1). In panels (a) and (b) of Fig. 1, the cut along the line $y=0$ is plotted, in panel (c) the cut is shown along the $x = X-$point. Near the X-point, where both the magnetic field and in-plane electron flow are zero, we

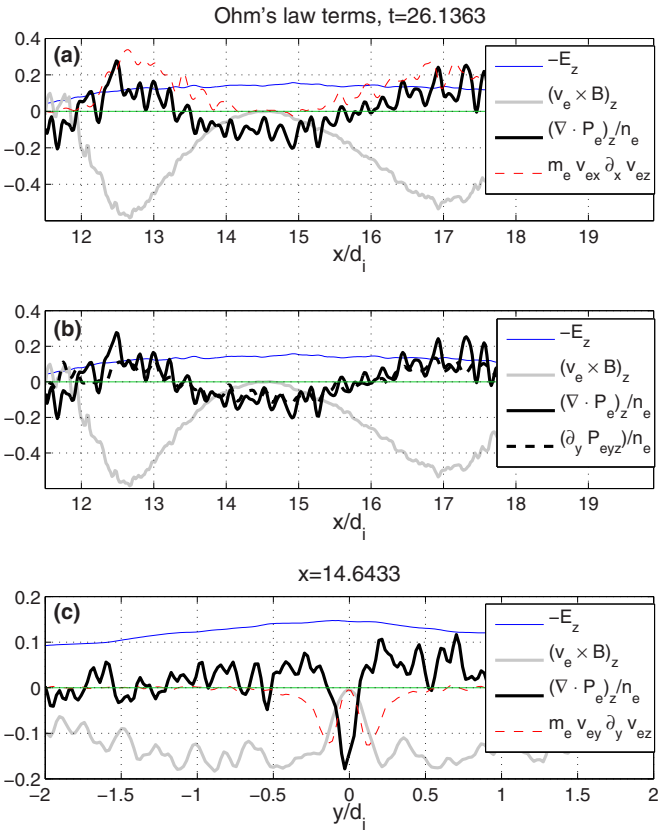

FIG. 1. (Color online) [(a) and (b)] Ohm's law terms along the $y=0$ line and (c) along the $x = X-$point line at $\Omega_{i0} t = 26.1$. The prevalence of $(\nabla \cdot \mathbf{P})_z$ over the convective term $(\mathbf{v} \times \mathbf{B})_z$ marks the EDR extent. The collisionless dissipation inside the EDR is provided mostly by $\partial_y P_{eyz}/n_e$ term [dotted line in panel (b)] attributed to electron thermal inertia.

can neglect the convective term $(\mathbf{v}_e \times \mathbf{B})_z$ and the bulk flow inertia term $(\mathbf{v}_e \nabla)\mathbf{v}_e$. The pressure gradient $\nabla \cdot \mathbf{P}_e$ compensates the electric field E_z at this point.[17,19]

The particle distribution functions in the $v_y - v_z$ plane are plotted in Fig. 2. Particles are separated into "accelerated" and "inflowing" populations by means of the following algorithm:

- The distribution function is sampled inside the EDR close to the X-point [see Fig. 2, panel (h)] at time t_0 (when steady state is presumably reached).
- Because the electron trapping time scale in the EDR is much smaller than any global time scale, the particle trajectories are numerically integrated with a $\mathbf{E}(\mathbf{x}, t_0)$, $\mathbf{B}(\mathbf{x}, t_0)$ fixed configuration.
- The number M_c of crossings of a trajectory with the $y=0$ plane are counted. For particles located at $y > 0$, M_c could be 0 (a particle never crossed the DR and is magnetized, blue in Fig. 2) or 1 (particle is from the $y < 0$ half-space and is being unmagnetized, green in Fig. 2). For particles from $y < 0$ half-space, M_c could be 0 (green in Fig. 2) or 1 (particle is from the $y > 0$ half-space and is being unmagnetized, blue in Fig. 2). Particles with $M_c > 1$ belong to the accelerated particle population (red in Fig. 2) at both half-spaces. In the rest of the paper, we call the particles with $M_c = 1$ as inflowing for the sake of simplicity.

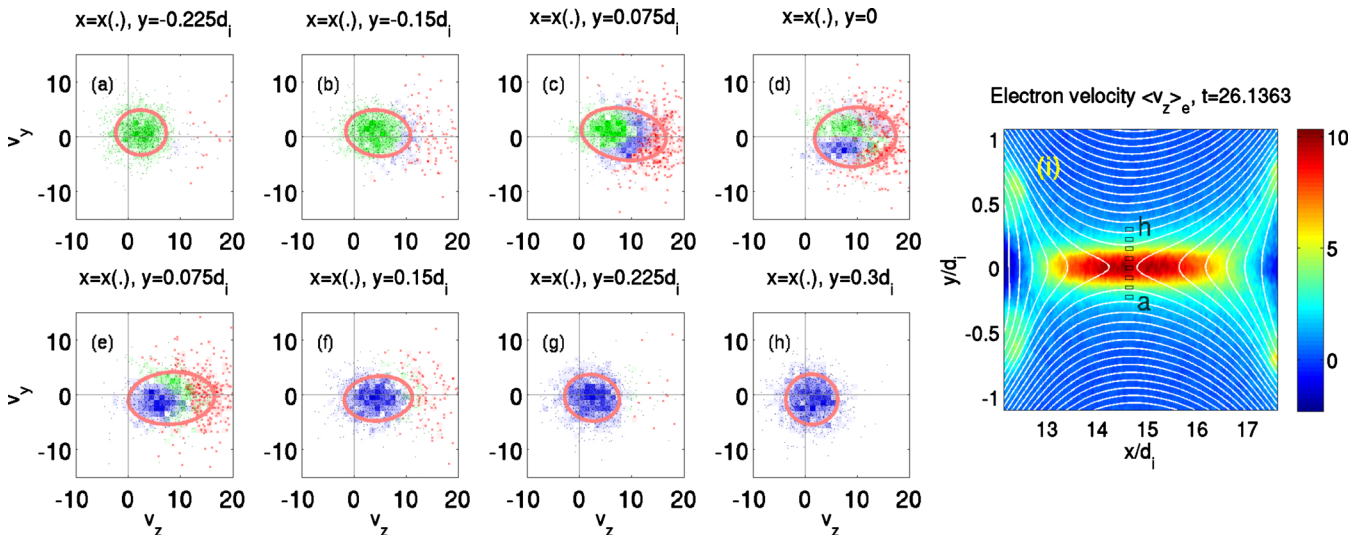

FIG. 2. (Color online) [(a)–(h)] Electron distribution functions in the EDR. Blue-colored (green-colored) particles constitute the population of particles inflowing from top (bottom) half-space. Red-colored particles represent the accelerated population. Distribution functions are sampled along the line crossing the EDR parallel to the $\hat{\mathbf{y}}$ axis. The red circle represents a contour of Maxwellian distribution (at 20% of a peak level) with velocity and pressure equal to that of a sampled distribution. (i) Out-of-plane electron flow velocity v_{ez} with superimposed magnetic field lines. The small boxes enclose the areas, where the electron distribution function is sampled.

The off-diagonal component P_{yz} appears in Fig. 2 as a correlation between the v_y and v_z velocities. Such correlation is clear at the top and bottom EDR edges [panels (b) and (c) and (e) and (f)], making P_{yz} nonzero there. Closer to $y\sim 0$, a symmetric inflow from both half-spaces makes $P_{yz}\sim 0$ with clearly non-Maxwellian distribution [panel (d)]. Variation of P_{yz} along the $\hat{\mathbf{y}}$ direction creates a nonvanishing $\partial P_{yz}/\partial y$ in the Ohm's law, leading to collisionless electron dissipation.

The electron density fluctuates negligibly across the EDR [Fig. 3, panel (a), red dashed line]. Almost all particles are drifting on the EDR edges ($y\sim 7.3d_i$ and $y\sim 7.7d_i$), while both populations are significant inside the EDR [see Figs. 2(c)–2(e)]. The density of accelerated particles peaks there at $\sim$30% of the total electron density [Fig. 3, panel (a)], with a slight dip immediately at the X-line.

The inflowing particles are distributed symmetrically around the v_y axis at the edge of the EDR [see Fig. 2, panel (h)], where accelerated particles are absent. We observe that closer to the X-line, f_d is shifted in the v_z direction either by the $\nabla\mathbf{B}$ drift of particles in decreasing $\mathbf{B}$ field or by the acceleration of particles by the reconnection electric field E_z [Figs. 2(a)–2(g)]. Thus, the symmetry condition (9), which we used to derive P_{yz}, is not exact.

However, a more general property of the electron distribution function $\langle v_y v_z\rangle_e=0$ is true at least for the inner part of the EDR [see Fig. 3, panel (b)]. Thus, Eqs. (13) and (14) provide a good estimate for the off-diagonal pressure component P_{yz}. Profiles are plotted for $x=X-$point [see Fig. 3, panel (b)].

These results confirm that the electron distribution function in the EDR could be represented as a superposition of drifting inflowing f_d and accelerated f_a distribution functions. An algorithm is presented which divides the particles in different classes in PIC simulations of antiparallel reconnection. The population of inflowing particles is found not to

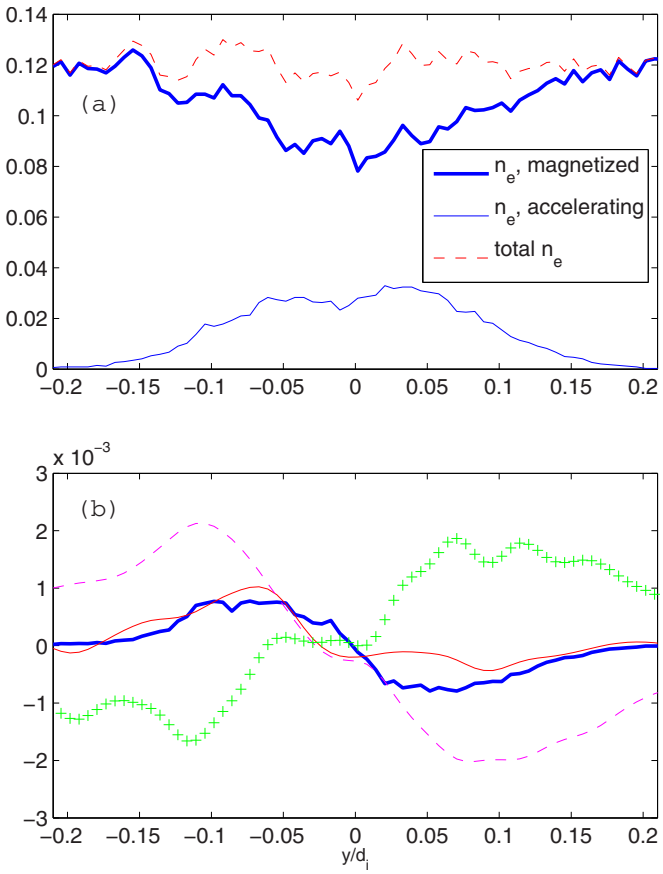

FIG. 3. (Color online) (a) Density of different electron populations: inflowing n_d (thick blue line), accelerated n_a (thin blue line), and total n_e (red dashed line). (b) Momentum transport across the X-line. P_{yz} (red thin line), $m_e n_e\langle v_y\rangle_e\langle v_z\rangle_e$ approximation (purple dashed line), P_{yz} approximation [Eq. (14)] based on trajectory separation (blue thick line), $m_e n_e\langle v_y v_z\rangle_e$ term (green crosses).

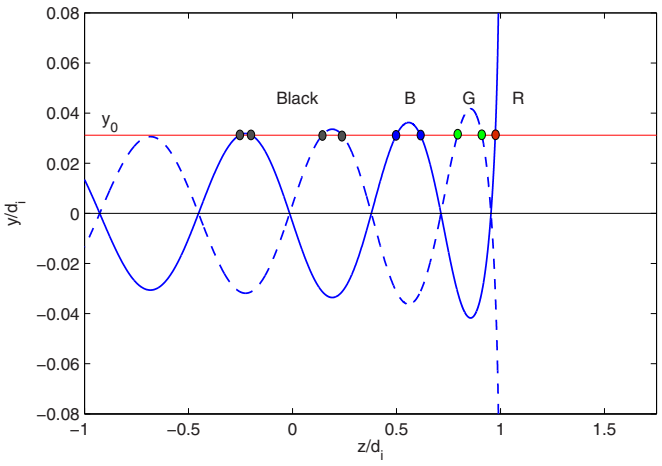

FIG. 4. (Color online) Trajectory of particles (y-z plane) drifting in the field-reversal with $v_{th}=0$ at $t=0$. At a point $y=y_0$, inflowing particles are observed (R) as well as those particles which crossed $y=0$ plane once (G), twice (B), and multiple (black) times.

be strictly symmetric around the v_y axis as it has been emphasized in Sec. II, but the condition $\langle v_y v_z \rangle_e = 0$ holds there.

IV. CASE OF COLD PLASMA: TEST-PARTICLE APPROACH

Specific symmetric properties of the distribution functions (inflowing and accelerated populations) were assumed in our derivation: the distribution function of inflowing particles is symmetric in the v_y direction while the distribution function of accelerating particles is symmetric in the v_z direction. These properties are satisfied in average sense if the particle thermal spread is introduced. Such symmetric properties are not fulfilled in the case of a cold plasma. This case was investigated by Fujimoto and Sydora in Ref. 28 (we call this model "Ladybug model" because of peculiarity of its electron distribution function, see Fig. 3 of their work[28]).

It is evident that the Ladybug model[28] is correct for the case of cold electrons, $v_{th}=0$. For this case, the motion of the inflow and meandering/accelerating particles proceeds along the curve in the phase space ($\mathbf{x}-\mathbf{v}$) without thermal dispersion (Fig. 4), leading to a spot-like structure of the distribution function (see Fig. 5). Inflowing particles are labeled with a red dot; green dots represent the population of particles that crossed once the $y=0$ plane, blue dots represent particles which experienced two crossings of the $y=0$ plane, and all other particles are colored black (Fig. 4). For the one-dimensional test-particle case, the accelerating particles are not removed from the system.

We can see from Fig. 5 that dots are distributed along the curves which are symmetric around the $v_y=0$ line. Nevertheless, separate dots are shifted by a typical Δv_z velocity, which is the velocity the particles gain in one meandering oscillation. If the thermal energy of the inflowing particle is more than this energy gains, then the symmetry conditions we assumed are valid, and our expression (14) determines the pressure anisotropy.

This result is in agreement with the approach in Ref. 28 and with the proposed model. To verify this, we introduce a finite thermal spread to the Ladybug model and study its influence on the distribution functions and on the P_{yz} component of the pressure tensor.

We limit ourselves to the numerical integration of the particle trajectories in a fixed one-dimensional field-reversal configuration because the task is highly complex to solve analytically.[13,14,42] Electrostatic effects are omitted. A relatively thin current sheet, $L=0.4d_i$, is chosen. Mass ratio $m_i/m_e=100$ and reconnection electric field $E_z=-0.1V_aB_0$ are taken from the Fujimoto and Sydora[28] article. Velocities are normalized to the Alfvén velocity.

The trajectories of $N=2000$ particles are calculated. The initial coordinate of all particles is $y=1d_i$ and the thermal velocities at different cases are $v_{th}=0$, $v_{th}=0.5V_a$, $v_{th}=3V_a$, and $v_{th}=15V_a$. The initial bulk flow velocity of particles corresponds to the $\mathbf{E}\times\mathbf{B}$ drift velocity at $y=1d_i$. The distribution functions and their moments are sampled within the segment $[y, y+\Delta y]$, where a small $\Delta y=10^{-3}d_i$ was used. Because there is no sink of particles in the one-dimensional calculation, the integration is stopped at a time t_{max}, which approximately represents 20 bounce periods of unmagnetized particles.

The distribution functions of particles in the v_y-v_z space are plotted in Fig. 5 ($v_{th}=0$) and Fig. 6 (different values of initial v_{th}). The amplitude of the meandering oscillations[27] λ, based on thermal velocity v_{th} and L, is larger than the initial thermal electron gyroradius ρ_{eth} and is $0.04d_i$, $0.1d_i$, and $0.25d_i$ (for the initial thermal velocities $v_{th}=0.5V_a$, $v_{th}=3V_a$,

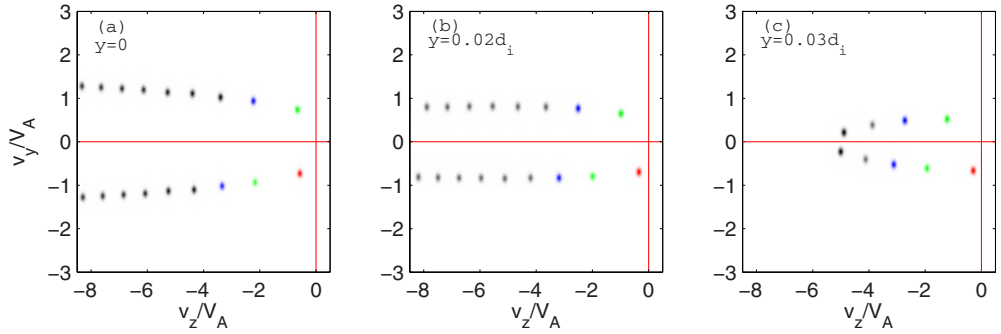

FIG. 5. (Color online) Particle distribution function in the v_y-v_z space obtained with a test-particle calculation with $v_{th}=0$ in a fixed field-reversal configuration and uniform E_z. Colors are set according to Fig. 4. Panel (b) displays a distribution function that is very close to the one used in the Ladybug model (Ref. 28).

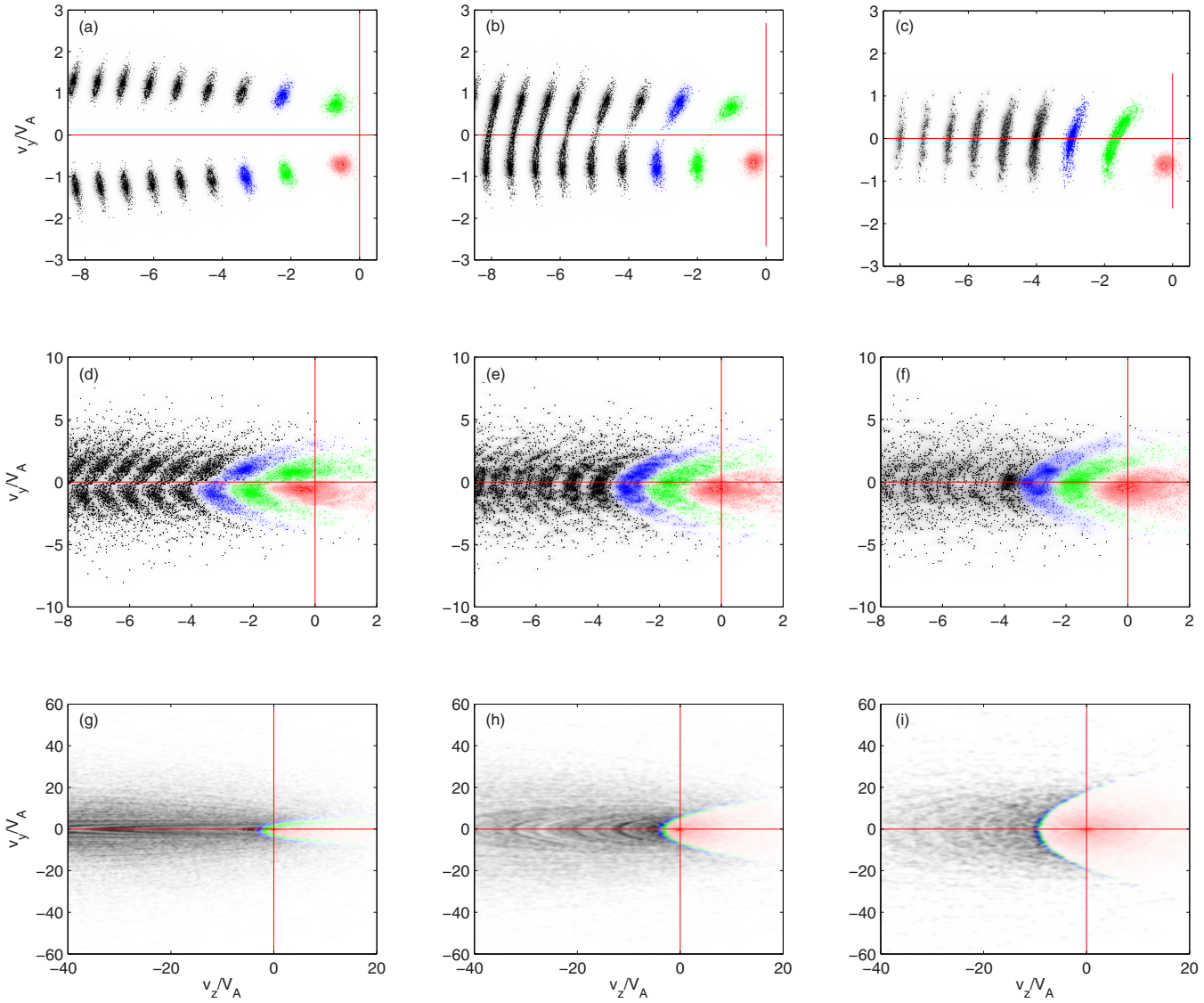

FIG. 6. (Color online) Electron distribution function in the v_y-v_z space computed with test-particle calculation for different thermal velocities of inflowing plasma: [(a)–(c)] $v_{\rm th}=0.5V_a$, [(d)–(f)] $v_{\rm th}=3V_a$, [(g)–(i)] $v_{\rm th}=15V_a$. At smaller thermal velocities, separate meandering spots are still visible, whereas all the accelerating particles cover the v_y-v_z space continuously at higher thermal velocities.

and $v_{\rm th}=15V_a$, correspondingly). We readily see that the number of accelerating particles is large within the segment $0<y<\lambda$. Particles are colored according to their meandering period similar to Figs. 4 and 5 (the $v_{\rm th}=0$ case). Even for the case of relatively cold inflow particles [Fig. 6, panels (a)–(c)], we observe the merging and stretching of areas in the v_y-v_z space, occupied by accelerating particles of different meandering periods. For the case of $v_{\rm th}=3V_a$ [Figs. 6(d)–6(f), with the simulation parameters similar to those of Ref. 28], the stretching is even more pronounced and separate spots are extended into a chain of adjacent "C"-shaped patterns. For $v_{\rm th}=15V_a$ [Fig. 6, panels (g)–(i)] separate meandering periods become poorly distinguishable and we readily see that the division into two particle populations (inflowing and accelerating) provides the correct description of the whole electron population. In realistic two- or three-dimensional configuration, particles reside in the field-reversal for some limited time before the ejection. Thus, the concentration of accelerated particles should be much smaller in realistic configuration compared to the results of one-dimensional calculations. This is clear by comparing directly Fig. 2 (PIC simulation) and Fig. 6 (one-dimensional calculation).

The presented calculations show how the Ladybug model changes by increasing the temperature of the inflowing particles. We confirm that the particle oscillations create spot-like distribution functions in a field-reversal in the cold plasma case. For high enough temperatures, these spots diffuse and merge into a uniform population of accelerated particles. The distribution functions, which consist of just two populations (inflowing and accelerated), are discussed in our model of the pressure anisotropy, hence the conclusion is that both models describe pressure anisotropy correctly. The Ladybug model is applicable to relatively cold plasma ($v_{\rm th}\sim 0$), and our model describes the case of hot plasma ($v_{\rm th}>0$). However, the question is still open how the models are related in strict physical and analytical sense. A more

accurate theory will account for both meandering oscillation of particles and thermal spread of distribution functions.

V. SUMMARY

The electron pressure anisotropy in the inner EDR is studied in this paper. The gradient of this anisotropic pressure balances the reconnection electric field E_z in the absence of other collisionless dissipative effects (for example, wave-particle interaction or small-scale turbulence). A simple analytical estimate for the P_{yz} component is obtained: given a distribution function inside the EDR which satisfies the condition $\langle v_y v_z \rangle_e \sim 0$, Eqs. (13) and (14) provide a reasonable P_{yz} estimate.

Such distribution functions could be easily constructed if it is assumed that all particles close to the X-line fall into two broad categories: inflowing particles and accelerated particles. By assuming the general symmetry properties of the distribution functions of these different populations [see Eqs. (9) and (10)], the term $\langle v_y v_z \rangle_e$ can be neglected and the formula $P_{yz}=m_e n_e \langle v_y \rangle_e \langle v_z \rangle_e$ can be used.

In addition, PIC simulations verified our theoretical conclusions. The closures for P_{yz} are in good agreement with the simulation results within the EDR if the $\langle v_y v_z \rangle_e \sim 0$ condition is partially satisfied. However, the $\langle v_y v_z \rangle_e \sim 0$ equation is determined exclusively by the distribution function symmetry we assumed. Close to the X-line, where both accelerated and inflowing populations are significant, the distribution function of inflowing particles is shifted in the v_z direction because of the gradient drift or demagnetization in weak magnetic field. We conclude that a more detailed investigation of the electron demagnetization and acceleration inside the EDR is required.

An extensive comparison of our model to the one developed in Ref. 28 is performed. Both approaches are based on similar principles:

(1) The electrostatic effects, the ion dynamics, and two- and three-dimensional effects are neglected.
(2) The electron anisotropy results from the particle acceleration by the reconnection electric field.
(3) The derivation of P_{yz} is based on the analysis of the particle trajectories. The resulting expressions are comparable in both models.

However, we point out the following important differences:

(1) The Ladybug model is derived for absolutely cold plasma. We qualitatively reconcile that approach with our model. Trajectories of a set of particles in a fixed field-reversal are integrated numerically and the distribution functions for different thermal velocities of inflowing plasma are collected. Separate spots are smoothed into C-shaped patterns as the temperature increases, and then merge into a uniform accelerated population at higher temperatures, thus reproducing our model.
(2) The pressure anisotropy is created by the $m_e n_e \langle v_y v_z \rangle_e$ term, as the inflow velocity $\langle v_y \rangle_e$ is zero deep inside the EDR at the stagnation point. The final expression for P_{yz} is similar to our results if some effective velocity (i.e., the velocity of inflowing particles) is taken instead of zero $\langle v_y \rangle_e$. However, our numerical simulations clearly indicate that $\langle v_y v_z \rangle_e$ could be neglected near the X-line for the case of $v_{th} > 0$.

We conclude here that pressure anisotropy develops in slightly different ways for plasmas with $v_{th}=0$ or $v_{th}>0$ and a more general picture will include both cases. This question will be a matter of further investigations.

ACKNOWLEDGMENTS

The present work is supported partially by the Onderzoekfonds KU Leuven (Research Fund KU Leuven) and by the European Commission's Seventh Framework Programme (FP7/2007-2013) under grant Agreement No. 218816 (SOTERIA project, www.soteria- space.eu). Additional support is provided by RFBR (Grant No. 09-05-91000-ANF-a). V.S.S. thanks ISSI for hospitality and financial support. The simulations were conducted on the resources of the Vlaams Supercomputer Centrum (VSC) at the Katholieke Universiteit Leuven.

[1] E. R. Priest and T. Forbes, *Magnetic Reconnection: MHD Theory and Applications* (Cambridge University Press, Cambridge, 2000), p. 600.
[2] D. Biskamp, *Magnetic Reconnection in Plasmas* (Cambridge University Press, Cambridge, 2000).
[3] P. Sweet, Il Nuovo Cimento **8**, 188 (1958).
[4] E. N. Parker, Astrophys. J., Suppl. Ser. **8**, 177 (1963).
[5] A. A. Galeev and R. Z. Sagdeev, in *Basic Plasma Physics: Selected Chapters, Handbook of Plasma Physics*, edited by A. A. Galeev and R. N. Sudan (North-Holland, Amsterdam, 1984), Vol. 1, p. 271.
[6] F. V. Coroniti, Space Sci. Rev. **42**, 399 (1985).
[7] J. Büchner and L. M. Zelenyi, J. Geophys. Res. **92**, 13456, doi:10.1029/JA092iA12p13456 (1987).
[8] R. Numata and Z. Yoshida, Phys. Rev. Lett. **88**, 045003 (2002).
[9] M. A. Shay and J. F. Drake, Geophys. Res. Lett. **25**, 3759, doi:10.1029/1998GL900036 (1998).
[10] D. Biskamp, E. Schwarz, and J. F. Drake, Phys. Rev. Lett. **75**, 3850 (1995).
[11] M. Hoshino, T. Mukai, T. Terasawa, and I. Shinohara, J. Geophys. Res. **106**, 25979, doi:10.1029/2001JA900052 (2001).
[12] M. Hoshino, J. Geophys. Res., [Space Phys.] **110**, A10215, doi:10.1029/2005JA011229 (2005).
[13] S. V. Bulanov and P. V. Sasorov, Sov. Astron. **19**, 464 (1976).
[14] R. W. Moses, J. M. Finn, and K. M. Ling, J. Geophys. Res. **98**, 4013, doi:10.1029/92JA02267 (1993).
[15] J. Birn, J. F. Drake, M. A. Shay, B. N. Rogers, R. E. Denton, M. Hesse, M. Kuznetsova, Z. W. Ma, A. Bhattacharjee, A. Otto, and P. L. Pritchett, J. Geophys. Res. **106**, 3715, doi:10.1029/1999JA900449 (2001).
[16] W. Daughton, J. Scudder, and H. Karimabadi, Phys. Plasmas **13**, 072101 (2006).
[17] H. Karimabadi, W. Daughton, and J. Scudder, Geophys. Res. Lett. **34**, L13104, doi:10.1029/2007GL030306 (2007).
[18] T. D. Phan, J. F. Drake, M. A. Shay, F. S. Mozer, and J. P. Eastwood, Phys. Rev. Lett. **99**, 255002 (2007).
[19] M. A. Shay, J. F. Drake, and M. Swisdak, Phys. Rev. Lett. **99**, 155002 (2007).
[20] J. F. Drake, M. A. Shay, and M. Swisdak, Phys. Plasmas **15**, 042306 (2008).
[21] V. M. Vasyliunas, Rev. Geophys. **13**, 303, doi:10.1029/RG013i001p00303 (1975).
[22] J. W. Dungey, La Recherche Spatiale **2**, 15 (1989).
[23] L. R. Lyons and D. C. Pridmore-Brown, J. Geophys. Res. **95**, 20903, doi:10.1029/JA095iA12p20903 (1990).
[24] H. J. Cai, D. Q. Ding, and L. C. Lee, J. Geophys. Res. **99**, 35, doi:10.1029/93JA02519 (1994).

[25]M. Hesse and D. Winske, J. Geophys. Res. **99**, 11177, doi:10.1029/94JA00676 (1994).
[26]R. Horiuchi and T. Sato, Phys. Plasmas **4**, 277 (1997).
[27]M. M. Kuznetsova, M. Hesse, and D. Winske, J. Geophys. Res. **105**, 7601, doi:10.1029/1999JA900396 (2000).
[28]K. Fujimoto and R. D. Sydora, Phys. Plasmas **16**, 112309 (2009).
[29]M. Hesse, S. Zenitani, M. Kuznetsova, and A. Klimas, Phys. Plasmas **16**, 102106 (2009).
[30]M. M. Kuznetsova, M. Hesse, and D. Winske, J. Geophys. Res. **103**, 199, doi:10.1029/97JA02699 (1998).
[31]I. J. D. Craig and P. G. Watson, Phys. Plasmas **12**, 012306 (2005).
[32]D. A. Uzdensky and R. M. Kulsrud, Phys. Plasmas **13**, 062305 (2006).
[33]D. B. Korovinskiy, V. S. Semenov, N. V. Erkaev, A. V. Divin, and H. K. Biernat, J. Geophys. Res., [Space Phys.] **113**, A04205, doi:10.1029/2007JA012852 (2008).
[34]M. Hesse and J. Birn, J. Geophys. Res. **97**, 3965, doi:10.1029/91JA03003 (1992).
[35]G. R. Burkhart, J. F. Drake, and J. Chen, J. Geophys. Res. **95**, 18833, doi:10.1029/JA095iA11p18833 (1990).
[36]G. R. Burkhart, J. F. Chen, and J. F. Drake, J. Geophys. Res. **96**, 11539, doi:10.1029/91JA00893 (1991).
[37]G. E. Vekstein and E. R. Priest, Phys. Plasmas **2**, 3169 (1995).
[38]S. Markidis, G. Lapenta, and Rizwan-uddin, Math. Comput. Simul. **80**, 1509 (2010).
[39]G. Lapenta, S. Markidis, A. Divin, M. Goldman, and D. Newman, Phys. Plasmas **17**, 082106 (2010).
[40]J. U. Brackbill and D. W. Forslund, J. Comput. Phys. **46**, 271 (1982).
[41]E. G. Harris, Il Nuovo Cimento **23**, 115 (1962).
[42]T. W. Speiser, J. Geophys. Res. **70**, 4219, doi:10.1029/JZ070i017p04219 (1965).